Sensors and Materials, Vol. 35, No. 5 (2023) 1631–1645
MYU Tokyo

S & M 3276

Diagnosis of Nonlinear Lamb Wave Characteristics of Closed Microcrack in Plates

Hanfei Zhang,[1*] Maochao Lv,[2**] and Yanyan Luo[1]

[1]Information Service and Information Research Center, Huaiyin Normal University, No. 111, Changjiang West Road, Huai'an City, Jiangsu 223300, China
[2]Thermal Testing Department, Huai'an Measurement and Testing Center, No. 111, Changjiang West Road, Huai'an City, Jiangsu 223300, China

(Received January 7, 2023; accepted April 5, 2023)

Keywords: Lamb wave, wave structure loading method, second harmonic, nonlinear coefficient

In this study, we examined the nonlinear ultrasonic effect of closed microcracks in industrial plates and derived the relationship between the nonlinear coefficient and the characteristic parameters of closed microcracks by analyzing the contact nonlinear ultrasonic theoretical model. Firstly, we established the finite element mesh model of closed microcracks in an industrial aluminum plate by simulation analysis and excited the S1 mode Lamb wave in the plate by the wave structure loading method based on the dispersion curve of the material's nonlinear matching. Secondly, we set up sensor nodes to collect the signal after the interaction between the S1 mode Lamb wave and the closed microcracks. Finally, we preprocessed the signal to analyze the rule of the change in the level of interaction between the closed microcracks and the S1 mode Lamb wave depending on the characteristics. Experimental results show that the second-harmonic amplitude and nonlinear coefficient decrease with increasing crack width for the closed microcracks, but increase with increasing crack length. These results confirm the effectiveness of the contact nonlinear ultrasonic theoretical model.

1. Introduction

The ultrasonic guided wave method is one of the widely used structural damage detection methods. The propagation characteristics of ultrasonic guided waves are closely related to the elastic characteristics and microstructure of the medium. The structure and performance of the medium can be evaluated by extracting and analyzing the ultrasonic information. In particular, in large plates or tubular media, ultrasonic guided waves can travel far along the axial direction. The ultrasonic guided wave signal collected at a limited receiving position can reflect the characteristics of the medium in the whole propagation range. Compared with the traditional ultrasonic detection technology, the ultrasonic guided wave has the advantages of speed and high efficiency. It has become a research hotspot in the field of nondestructive testing in recent years.[1–4]

*Corresponding author: e-mail: zhanghanfei2006@163.com
**Corresponding author: e-mail: 270864278@qq.com
https://doi.org/10.18494/SAM4306

ISSN 0914-4935
https://myukk.org/

The traditional ultrasonic detection technology is developed on the basis of the theory of linear acoustics, which is characterized by linearizing the nonlinear acoustic equation under the assumption of small-amplitude acoustic waves. Nonlinear ultrasonic detection technology has high sensitivity to the microstructure characteristics of materials whose space size is much smaller than the ultrasonic wavelength. It has special advantages in the evaluation and detection of the early performance degradation of materials and early damage inside structures. Both geometric and material nonlinearities in the structure can cause the variation of nonlinear components in Lamb wave signals. Changes in the characteristic parameters of the nonlinear signal in the Lamb wave can be used for the early detection of the structural change caused by microcracks.[5,6] In a solid structure, acoustic particle vibration propagates in accordance with the stress–strain criterion, and the amplitude of the acoustic wave determines the rule of particle vibration. A particle vibration with small amplitude follows the linear proportional relationship between stress and strain, while a particle vibration with large amplitude shows a nonlinear phenomenon.[7] Although the classical nonlinear coefficient (inherent nonlinearity of the material) based on the ratio of fundamental and harmonic amplitudes can be used to describe the performance changes caused by a microcrack in a material, the propagation characteristics of a nonlinear ultrasonic wave become complicated owing to the diversity of microcracks. When the ultrasonic wave encounters contact damage (such as a closed microcrack) in the structure, friction and collision phenomena are generated. The higher-order harmonic energy changes again, making its energy much higher than that in the classical nonlinear ultrasonic theory. The classical nonlinear coefficient cannot be simply used to characterize this type of damage.[8]

To solve this problem, many scholars began to study the mechanism behind nonlinear ultrasonic waves and microcracking, and put forward some nonlinear detection models, such as the physical and phenomenological models. The physical model discusses the effect of microcracks on the ultrasonic response in accordance with the microphysical mechanism and characterizes the mechanical properties of the crack in terms of the contact stiffness of the microcrack. The phenomenological model uses the equivalent model to characterize the evolution of microcracks and discusses the relationship between nonlinear effects and microcracks. Although these two models can characterize the relationship between microcracks and nonlinear ultrasonic waves, it is still necessary to further improve the research of closed microcracks and nonlinear ultrasonic effects, and the quantitative evaluation of closed microcracks. In view of the limitation of using linear Lamb waves to detect microcracks and the sensitivity of nonlinear Lamb waves, it is important to study methods of enhancing the nonlinear feature of ultrasonic Lamb waves for the early crack identification of plate components. There are still many problems to be studied, such as the quantitative relationship between crack characteristics and nonlinear Lamb wave signals, the method of analyzing nonlinear Lamb waves, and the method of extracting damage evaluation features.[9–11]

It is difficult to accurately manufacture closed microcracks of desired sizes in the experimental thin plates. The accuracy of the closed microcrack size is also difficult to guarantee, which had given rise to great obstacles to physical experimentation. Therefore, in this study, we examined the nonlinear Lamb wave effect of closed microcracks in the plate structure by finite element modeling (FEM) and simulation. We excited a single S1 mode Lamb wave by

the wave structure loading method and set up eight sensor nodes to simulate the position of the receiving sensor. By collecting the data of the excited S1 mode Lamb wave and the second-harmonic signal, we confirmed the second-harmonic accumulation effect and analyzed the variation of the nonlinear coefficient on changing the size of the microcracks.

2. Theoretical Model of Nonlinear Ultrasonic Effect on Closed Microcracks

Using the micro–hysteretic force–displacement relationship of a single microconvex, Aleshin and Van derived the macro–stress–strain constitutive equation of the whole material.[12] It is assumed that the microcrack has the characteristics of a plane crack. The azimuth angle φ and θ are used to represent the plane crack angle, $\psi(\theta, \varphi)$ is the normal distribution function, $a_{\theta\varphi}$ is the average width of an opening–closing crack, and A is the width of the crack contact surface when internal stress $\sigma = 0$. Then, the three-dimensional normal strain can be expressed as

$$\begin{aligned} \varepsilon_{yy} &= \gamma_{yy} + S_V \int_0^{\pi/2} d\theta \int_0^{\pi} d\varphi (a_{\theta\varphi} - A)\psi(\theta,\varphi)\sin^3\theta \sin^2\varphi \\ \varepsilon_{zz} &= \gamma_{zz} + S_V \int_0^{\pi/2} d\theta \int_0^{\pi} d\varphi (a_{\theta\varphi} - A)\psi(\theta,\varphi)\cos^2\theta \sin\varphi \end{aligned}, \tag{1}$$

where S_V is the total area of the crack and γ_{ii} is the lossless time tensor. One-dimensionally, the strain can be expressed as

$$\varepsilon = \gamma + S_V \int_0^{\pi/2} (a_\theta - A)\cos^2\theta \sin\theta d\theta, \tag{2}$$

where tensor $\gamma = \gamma_{zz}$.

Because of the existence of contact interfaces, the closed microcracks in platelike structures will open and close after encountering ultrasonic waves. This phenomenon can be described by the nonlinear spring model described below.[13]

Let the length of the plate be L and the thickness be D. A simple harmonic ultrasonic signal with angular frequency ω is excited on the plate and propagates along the length of the plate. Its displacement is x, and the displacement field can be expressed as

$$u_1(x,t) = U_1(x)\cos\omega t, \tag{3}$$

where $U_1(x)$ is the standing wave displacement field expressed as

$$U_1(x) = A_1 \cos k_1 x u_z. \tag{4}$$

Here, A_1 is the fundamental amplitude of the excitation signal and k_1 is the wave number.

Suppose that the closed microcrack is located at x_0 and its normal direction is parallel to x. w is the short axis of the crack (crack width) and l is the long axis of the crack (crack length). The internal stress in the contact surface can be expressed as

$$\sigma = E\varepsilon(1+\beta_0\varepsilon), \tag{5}$$

where E is Young's modulus, β_0 is the inherent nonlinear coefficient (classical nonlinear) of the material, and ε is the change in crack width.

According to Hertz contact theory, the contact depth h can be expressed as[14]

$$h = \left[\frac{9}{16}\left(\frac{1}{R}+\frac{1}{R'}\right)\left(\frac{1+\upsilon^2}{E}+\frac{1+\upsilon'^2}{E'}\right)^2 u_1^2\right]^{1/3}, \tag{6}$$

where E and E' are Young's moduli, υ and υ' are Poisson's ratios, and R and R' are curvatures.

Equation (6) shows that the contact depth of the closed microcrack is proportional to the amplitude of the excited sound wave.

Isotropic materials have the following characteristics:

$$E = E',\ \upsilon = \upsilon',\ R = R' = -\frac{w^2}{2l}.$$

The contact depth h can be expressed as

$$h = -\left[72\left(\frac{l}{w^2}\right)\left(\frac{1+\upsilon^2}{E}\right)^2 u_1^2\right]^{1/3}. \tag{7}$$

The width of the closed microcrack will change under the action of the excited sound wave, which can be expressed as

$$\begin{aligned}\varepsilon &= -\left[72\left(\frac{l}{w^2}\right)\left(\frac{1+\upsilon^2}{E}\right)^2 u_1^2\right]^{1/3}\frac{\partial u_1}{\partial x}\\ &= -\left[72\left(\frac{l}{w^2}\right)\left(\frac{1+\upsilon^2}{E}\right)^2 u_1^2\right]^{1/3}\frac{\partial U_1(x)}{\partial x}\cos\omega t.\end{aligned} \tag{8}$$

By substituting Eq. (8) into Eq. (5), the internal stress can be expressed as

$$\begin{aligned}\sigma = &-\left[72\left(\frac{l}{w^2}\right)\left(\frac{1+\upsilon^2}{E}\right)^2 u_1^2\right]^{1/3} E\frac{\partial U_1(x)}{\partial x}\Big|_{x=x_0}\cos\omega t \\ &+\frac{1}{2}\beta_0 E\left[72\left(\frac{l}{w^2}\right)\left(\frac{1+\upsilon^2}{E}\right)^2 u_1^2\right]^{2/3}\left(\frac{\partial U_1(x)}{\partial x}\right)^2\Big|_{x=x_0} \\ &+\frac{1}{2}\beta_0 E\left[72\left(\frac{l}{w^2}\right)\left(\frac{1+\upsilon^2}{E}\right)^2 u_1^2\right]^{2/3}\left(\frac{\partial U_1(x)}{\partial x}\right)^2\Big|_{x=x_0}\cos 2\omega t.\end{aligned} \tag{9}$$

By substituting Eq. (4) into Eq. (9), we can obtain

$$\begin{aligned}\sigma = &-\left[72\left(\frac{l}{w^2}\right)\left(\frac{1+\upsilon^2}{E}\right)^2 u_1^2\right]^{1/3} k_1 E A_1 \sin k_1 x_0 \cos\omega t \\ &+\frac{1}{2}\beta_0\left[72\left(\frac{l}{w^2}\right)\left(\frac{1+\upsilon^2}{E}\right)^2 u_1^2\right]^{2/3} k_1^2 E A_1^2 \sin^2 k_1 x_0 \\ &+\frac{1}{2}\beta_0\left[72\left(\frac{l}{w^2}\right)\left(\frac{1+\upsilon^2}{E}\right)^2 u_1^2\right]^{2/3} k_1^2 E A_1^2 \sin^2 k_1 x_0 \cos 2\omega t,\end{aligned} \tag{10}$$

where the third term on the right of Eq. (10) is the second-harmonic component contained in the internal stress, which can be expressed as

$$\Delta\sigma^{(2\omega)} = \frac{1}{2}\beta_0\left[72\left(\frac{l}{w^2}\right)\left(\frac{1+\upsilon^2}{E}\right)^2 u_1^2\right]^{2/3} k_1^2 E A_1^2 \sin^2 k_1 x_0 \cos 2\omega t. \tag{11}$$

The displacement field of the second harmonic is expressed as

$$u_2(x,t) = U_2(x)\cos 2\omega t, \tag{12}$$

where $U_2(x)$ is its standing wave displacement field expressed as

$$U_2(x) = \begin{cases} C_1 \cos k_2 x, & x < x_0 \\ C_2 \cos k_2 x(L-x), & x \geq x_0 \end{cases}. \tag{13}$$

Here, k_2 is the wave number of the second harmonic and C_1 and C_2 are undetermined coefficients. Equation (13) can be solved by applying the displacement and boundary conditions of the acoustic wave at the closed microcrack.

When the sound wave propagates to the crack, displacement and stress can be expressed as

$$U_2(x = x_0^-) = U_2(x = x_0^+), \tag{14}$$

$$\sigma^{(2\omega)}\Big|_{x=x_0^+} - \sigma^{(2\omega)}\Big|_{x=x_0^-} = \frac{2F^{(2\omega)}}{Dz_0}, \tag{15}$$

where z_0 is the length of the plate in the direction z and $F^{(2\omega)}$ is the internal stress corresponding to the second harmonic, which can be expressed as

$$F^{(2\omega)} = lz_0\Delta\sigma^{(2\omega)}. \tag{16}$$

The stress–strain relationship of the second-harmonic displacement field can be expressed as[15]

$$\sigma^{(2\omega)} = \frac{E}{1-\upsilon^2}\frac{\partial u_2}{\partial x}. \tag{17}$$

By integrating Eqs. (11)–(16) and solving Eq. (17), the second-harmonic displacement field can be obtained as

$$\begin{aligned} u_2(x,t) &= \left[72\left(\frac{l}{w^2}\right)\left(\frac{1+\upsilon^2}{E}\right)^2 u_1^2\right]^{2/3}(1-\upsilon^2)l\frac{\beta_0 k_1^2 A_1^2}{k_2 D}\left(\frac{\cos k_2 x_0}{\sin k_2 L}\right)\cos k_2(L-x)\cos 2\omega t \\ &= \frac{l^{5/3}}{w^{4/3}}A_1^2\left\{\left[72\left(\frac{1+\upsilon^2}{E}\right)^2 u_1^2\right]^{2/3}(1-\upsilon^2)\frac{\beta_0 k_1^2}{k_2 D}\frac{\cos k_2 x_0}{\sin k_2 L}\cos k_2(L-x)\right\}\cos 2\omega t. \end{aligned} \tag{18}$$

It can be concluded that the opening–closing action of a microcrack complicates the variation of the acoustic displacement field in the plate. The amplitude A_2 of the second harmonic is affected by the crack width, length, and amplitude of the fundamental wave, and the material and structural parameters of the plate. The relationships are as follows.

$$A_2 \propto \frac{l^{5/3}}{w^{4/3}}A_1^2 \tag{19}$$

Equation (19) shows that the ratio of the amplitude of the second-harmonic component to the square of the fundamental frequency amplitude can be used to describe the size of the microcrack. The ratio is represented by the contact nonlinear coefficient β.

$$\beta = \frac{A_2}{A_1^2} \tag{20}$$

Therefore, the nonlinear effect of ultrasonic waves in plate structural materials includes two parts: material inherent nonlinearity and contact nonlinearity. The unified nonlinear coefficient β' is expressed as

$$\beta' = \beta_0 + \beta. \tag{21}$$

Since $\beta_0 << \beta$, the default value is $\beta' \approx \beta$, and the nondestructive evaluation of closed microcracks can be carried out directly by using the contact nonlinear coefficient β.

3. Lamb Wave Dispersion Characteristics and Wave Structure Loading Method

The stress and displacement fields of the symmetrical mode Lamb wave in the isotropic plate are shown as Eqs. (22) and (24), respectively.

Symmetric mode:

$$\sigma_{zz} = -\lambda(k^2 - q^2)A_2 \cos(pz)] - 2\mu[p^2 A_2 \cos(pz) + ikqB_1 \cos(qz)], \tag{22}$$

$$\sigma_{xz} = \mu[-2ikpA_2 \sin(pz) + (k^2 - q^2)B_1 \sin(qz)], \tag{23}$$

$$u_z = -pA_2 \sin(pz) - ikB_1 \sin(qz)], \tag{24}$$

$$u_x = ikA_2 \cos(pz) + qB_1 \cos(qz)], \tag{25}$$

$$p^2 = \frac{\omega^2}{c_l^2} - k^2,\ q^2 = \frac{\omega^2}{c_s^2} - k^2, \tag{26}$$

$$A_2 = 2ikq\cos(qb),\ B_1 = (k^2 - q^2)\cos(pb). \tag{27}$$

Antisymmetric mode:

$$\sigma_{zz} = -\lambda(k^2 + q^2)A_1\sin(pz)] - 2\mu[p^2 A_1 \sin(pz) + ikqB_2 \sin(qz)], \tag{28}$$

$$\sigma_{xz} = \mu[2ikpA_1\cos(pz) + (k^2 - q^2)B_2 \cos(qz)], \tag{29}$$

$$u_z = -pA_1\cos(pz) - ikB_2 \cos(qz)], \tag{30}$$

$$u_x = ikA_1\sin(pz) - qB_2 \sin(qz)], \tag{31}$$

$$A_1 = 2ikq\sin(qb),\ B_2 = (q^2 - k^2)\sin(pb). \tag{32}$$

Here, x is the direction of Lamb wave propagation and z is the direction of plate thickness. When the wave number k_0 and angular frequency ω are substituted into the boundary conditions of the free plate ($\sigma_{xz} = \sigma_{zz} = 0$), the undetermined coefficients A_1, A_2, B_1, and B_2 can be obtained by substituting the wave number k_0 and angular frequency ω into the boundary conditions of the free plate ($\sigma_{xz} = \sigma_{zz} = 0$).

Furthermore, according to the nonlinear Lamb wave theory, only when the phase velocity of the fundamental Lamb wave matches the phase velocity of the second-harmonic Lamb wave does the relationship between nonlinear coefficient and propagation distance indicate linear growth.[16] Therefore, it is necessary to calculate the nonlinear matched dispersion curves of Lamb waves in the application of nondestructive detection and evaluation of the microcrack of a plate structure.[17]

4. Finite Element Modeling and Simulation

4.1 Damage model of plate and its nonlinear matching Lamb wave dispersion characteristics

Taking the isotropic aluminum plate as the research object, we carried out the finite element modeling and simulation analysis of the nonlinear Lamb wave effect of closed microcracks. The material is an AL-6061-T6 aluminum plate, and the material parameters are shown in Table 1, where ρ is the density, λ and μ are the second-order elastic constants (Lame constants), and L, M, and N are the third-order elastic constants.

The closed microcrack model is shown in Fig. 1. We set the closed microcrack at 40 mm on the left side of the plate. Its shape is an ellipse, the long axis is the length, and the short axis is the width. We set the plate length to 200 mm and the thickness to 2 mm. In the simulation experiment, we loaded the Lamb wave excitation signal from the left side of the board and set multiple sensor nodes on the board to receive the simulation signal at different positions. Therefore, it is necessary to set the ultrasonic excitation signal in accordance with the dispersion curve and plate structure parameters.

Table 1
Material parameters of AL-6061-T6 aluminum plate.

ρ (kg/m^3)		2704
Second-order elastic constants	λ (GPa)	67.6
	μ (GPa)	25.9
Third-order elastic constants	L (GPa)	−41.6
	M (GPa)	−131
	N (GPa)	−150.5

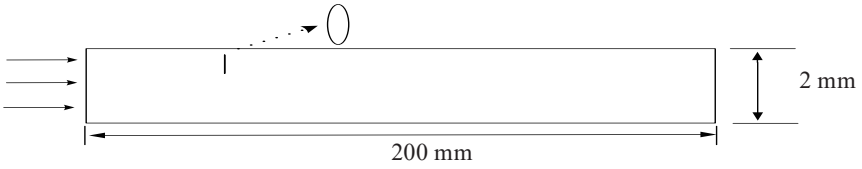

Fig. 1. Plate structure and its closed microcrack model.

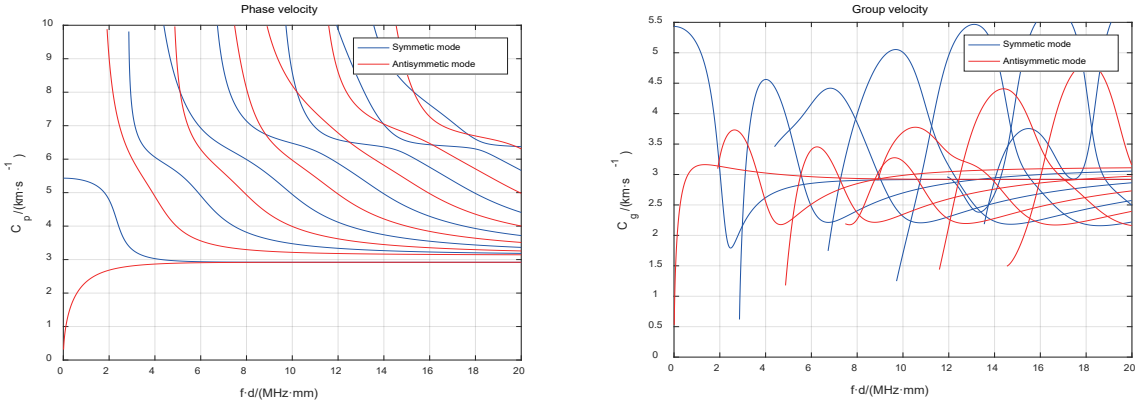

Fig. 2. (Color online) Lamb wave dispersion curve of aluminum plate. (a) Phase velocity dispersion curve. (b) Group velocity dispersion curve.

According to the dichotomy method, the Lamb wave dispersion curve of this type of aluminum plate is shown in Fig. 2. The blue curve is the symmetric mode, the red curve is the antisymmetric mode, and the abscissa is the frequency–thickness product ($f \bullet d$). Figure 2(a) shows the phase velocity and group velocity dispersion curves, and the ordinate is the phase velocity C_p. Figure 2(b) shows the group velocity dispersion curve, and the ordinate is the group velocity C_g.

Referring to the data in Fig. 2(a), we obtained the nonlinear matched phase velocity dispersion curve by selecting the S1 mode Lamb wave with a frequency of 1.895 MHz (plate thickness of 2 mm) as the excitation signal (fundamental wave), as shown in Fig. 3. The second harmonic is 3.79 MHz in the S2 mode and the third harmonic is 5.785 MHz in the S3 mode. Therefore, in the simulation experiment, we set the S1 mode Lamb wave excitation signal as a 15-period narrow-band sine wave signal with a frequency of 1.895 MHz with a Hanning window modulation.

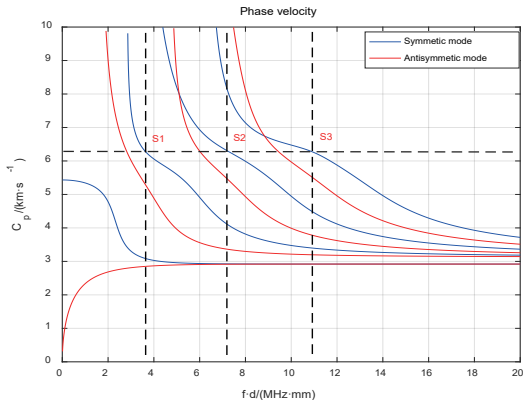

Fig. 3. (Color online) Nonlinear matched phase velocity dispersion curves.

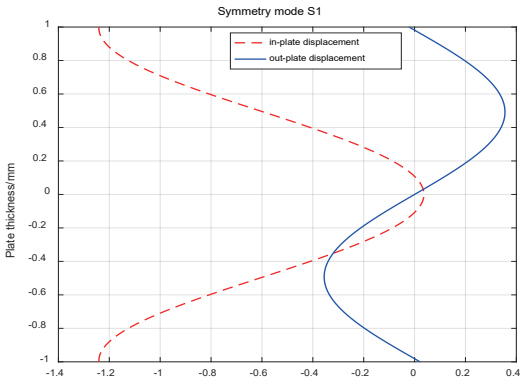

Fig. 4. (Color online) Wave structure curve of S1 mode Lamb wave.

The wave number and angular frequency can be determined from the dispersion curve. The wave structure curves of symmetric and antisymmetric mode Lamb waves can be obtained by using Eqs. (24), (25), (30), and (31), and they reflect the relationship between displacement and plate thickness. For the 2-mm-thick plate with the 1.895-MHz-frequency excitation signal, the wave structure curve of the S1 mode Lamb wave is shown in Fig. 4. The red curve is in-plane displacement and the blue curve is out-plane displacement. The abscissa is the direction of the wave vector and the ordinate is the direction of plate thickness.

In the finite element model, mesh generation is very important. Moser's group gave the grid computing criterion of finite element simulation, which depended on the wavelength of the excitation signal.[18] The maximum size of the grid depends on the phase velocity of the Lamb wave, and the following conditions should be satisfied:

$$\frac{\lambda_{min}}{\max(\delta x, \delta y)} > 20\,. \tag{33}$$

Here, λ_{min} is the minimum wavelength of the Lamb wave, δx is the distance between adjacent nodes in the x direction, and δy is the distance between adjacent nodes in the y direction. The calculation criterion of time step Δt is

$$0.7\frac{\min(\delta x, \delta y)}{c_g} \geq \Delta t. \tag{34}$$

On the basis of the above rules, we established the finite element simulation model for the plate structure and the closed microcrack damage model. The mesh generation of the model is shown in Fig. 5. The length of the plate is 200 mm and the thickness is 2 mm. Figure 5(a) shows the mesh of the undamaged area, and Fig. 5(b) that of the closed microcrack. By the wave structure loading method, we simulated and analyzed the nonlinear Lamb wave characteristics of the model.

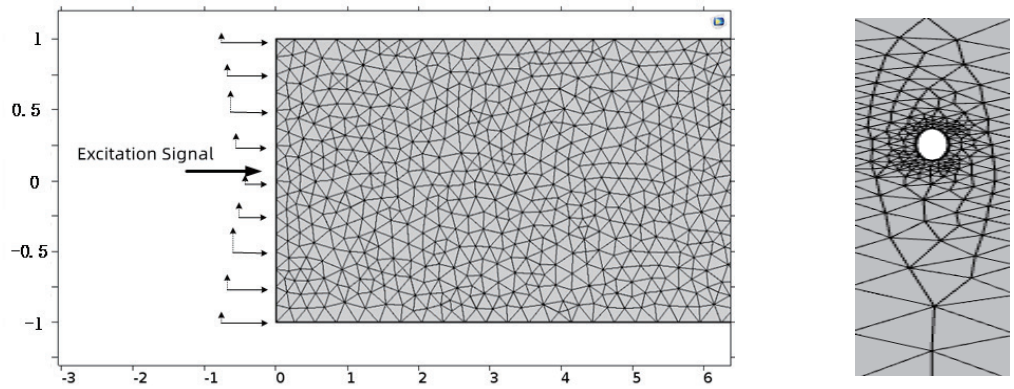

(a) (b)

Fig. 5. Finite element grid of closed microcrack model in plate. (a) No crack area. (b) Closed microcrack.

4.2 Simulation results and discussion

We set the closed microcrack 40 mm away from the left side of the plate and discussed the effects of the closed microcracks on the propagation of nonlinear Lamb waves in the two models with "the same width and different lengths" and "the same length and different widths". One model has a crack width of 4 μm and the lengths of 0.06, 0.09, 0.12, 0.15, 0.18, and 0.21 mm. The other model has a crack length of 0.09 mm and the widths of 2, 10, 40, 70, 100, and 130 μm.

We set up eight sensor nodes to simulate the position of the receiving sensor and collected the data of the excited S1 mode Lamb wave and the second-harmonic signal (the fundamental frequency is 1.895 MHz and the second-harmonic frequency is 3.79 MHz). The distances between the sensor nodes and the left boundary of the plate are 65, 70, 75, 80, 85, 90, 95, and 100 mm.

Firstly, we compared the received signals at each sensor node without and with a microcrack. Taking the sensor node at 70 mm as an example, Fig. 6 shows the time domain signal waveform, Fig. 7 shows the fundamental frequency spectrum, and Fig. 8 shows the second-harmonic frequency spectrum. The results show that the second-harmonic amplitude with a microcrack is higher than that without a microcrack.

Secondly, we analyzed the spectrum of the received signal at each sensor node without a microcrack, as shown in Fig. 9. The results show that the second-harmonic amplitude of the Lamb wave increases with the propagation distance in the crack-free case. This is consistent with the results of classical nonlinear ultrasonic theory that the second-harmonic amplitude increases with the propagation distance.[8] It is shown that the second harmonic of the Lamb wave has a cumulative effect under this condition, and the validity of using the S1 mode Lamb wave excited by the wave structure loading method is verified.

Furthermore, we analyzed the effect of the size of the closed microcrack on the propagation characteristics of nonlinear Lamb waves. To analyze the second-harmonic amplitude effectively, a high-pass filter was used to filter the received signal and retain the high-frequency components above the second harmonic. Taking the sensor node located at 70 mm as an example, we explored

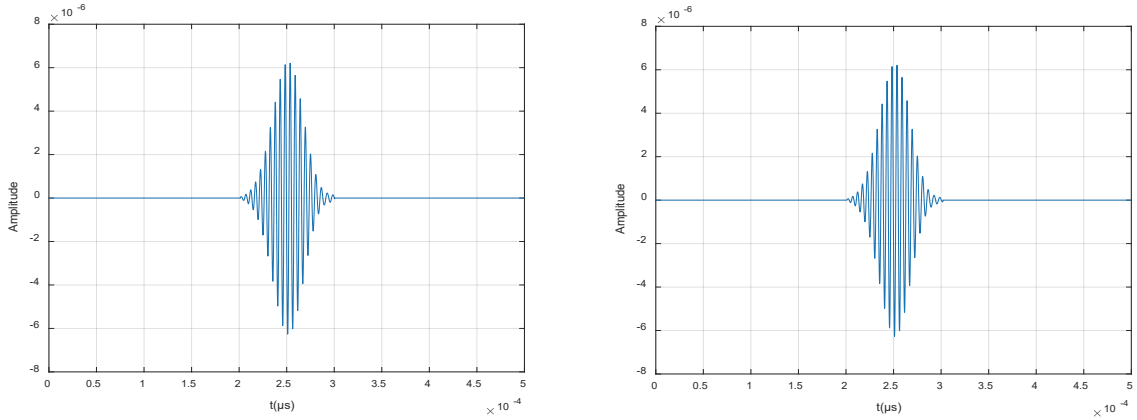

(a) (b)

Fig. 6. (Color online) Received signal waveform at node at 70 mm. (a) With microcrack. (b) Without microcrack.

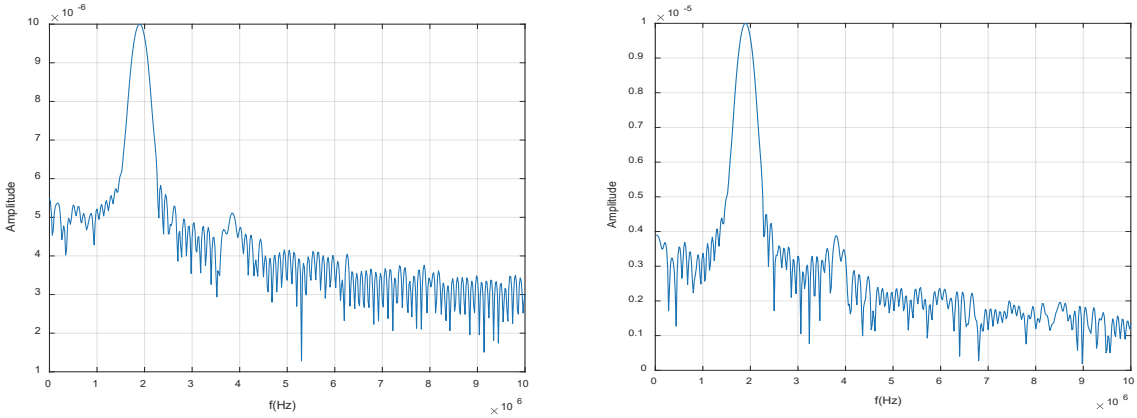

(a) (b)

Fig. 7. (Color online) Fundamental frequency spectrum of the received signal at node at 70 mm. (a) With microcrack. (b) Without microcrack.

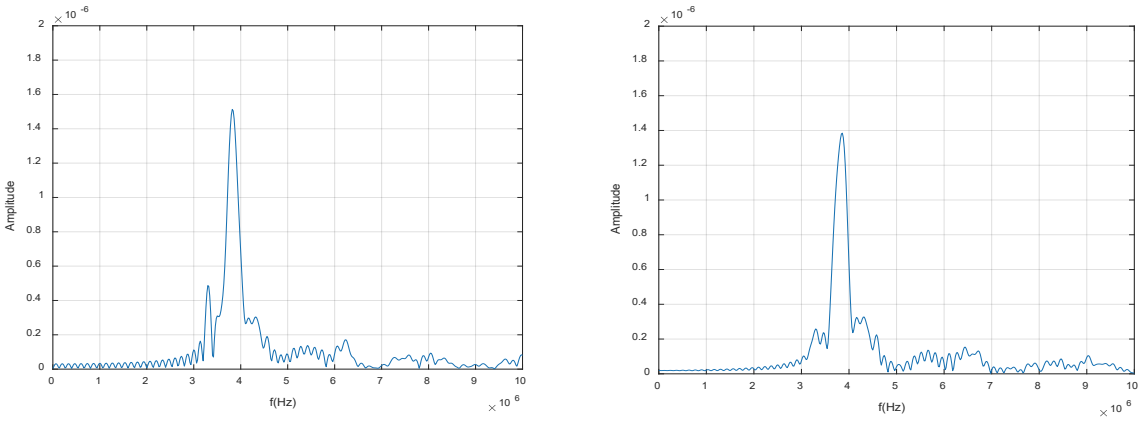

(a) (b)

Fig. 8. (Color online) Second-harmonic frequency spectrum of received signal at node at 70 mm. (a) With microcrack. (b) Without microcrack.

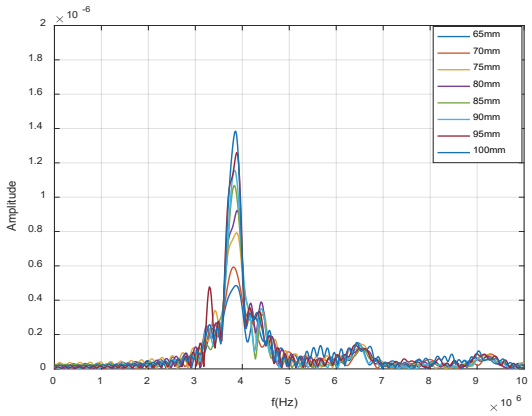

Fig. 9. (Color online) Second-harmonic spectrum at each node without microcrack.

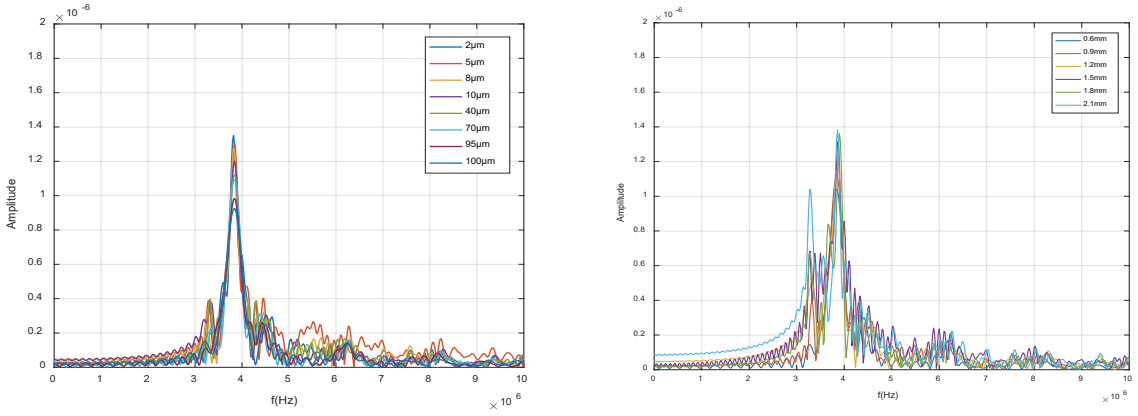

(a) (b)

Fig. 10. (Color online) Second-harmonic spectrum of received signal at node at 70 mm with different crack sizes. (a) 0.9 mm length and different widths. (b) 40 μm width and different lengths.

the relationship between the two types of mode cracks (0.9 mm length and different widths; 40 μm width and different lengths) and the second-harmonic spectrum. The results are shown in Fig. 10. The second-harmonic amplitude is directly related to the crack length and width. The second-harmonic amplitude decreases with increasing crack width, but increases with increasing crack length. This conclusion is consistent with Eq. (19).

Finally, we analyzed the variation of the contact nonlinear coefficient depending on the size (different widths and lengths) of the closed microcrack, as shown in Fig. 11. The results obtained at all eight receiving sensor nodes are presented. Figure 11(a) shows the relationship between the length of the crack and the nonlinear coefficient. Figure 11(b) shows the relationship between the width of the crack and the nonlinear coefficient. The results show that the nonlinear coefficient is related to both the length and width of the closed microcrack. The nonlinear coefficient decreases with increasing crack width, but increases with increasing crack length. This conclusion is consistent with Eq. (20). Therefore, the nonlinear coefficient can be used to characterize the change in closed microcrack size.

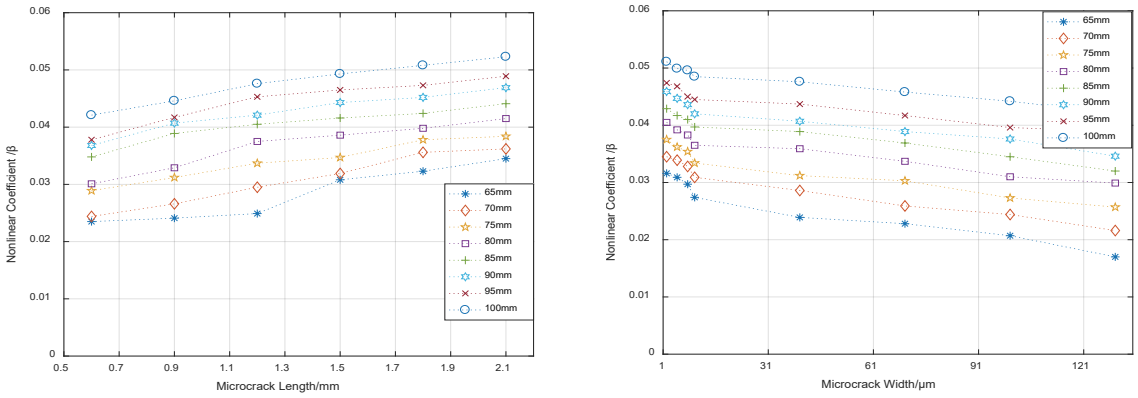

(a) (b)

Fig. 11. (Color online) Relationship between nonlinear coefficient and crack size at each node. (a) Relationship between crack length and nonlinear coefficient. (b) Relationship between crack width and nonlinear coefficient.

5. Conclusions

By theoretical model analysis and simulation, we studied the ultrasonic Lamb wave nonlinear effect in an aluminum plate with closed microcracks. We excited the S1 mode Lamb wave in the plate by the wave structure loading method, set up multiple sensor nodes to collect the closed microcrack damage signal, detected the higher-order mode signal, and analyzed the cumulative effect of the second harmonic and the effect of closed microcracks with different lengths and widths on the nonlinear coefficient. The results show that the second-harmonic amplitude increases with the propagation distance in the plate without microcracks. With closed microcracks, the second-harmonic amplitude and nonlinear coefficient decrease with increasing crack width and increase with increasing crack length. These results confirm the validity of the contact nonlinear ultrasonic theoretical model. The finite element simulation model based on this theory is helpful for analyzing the effect of closed microcracks on nonlinear Lamb wave characteristics in the plate, and the basic size characteristics of closed microcracks can be characterized by the second harmonic and the nonlinear coefficient.

Acknowledgments

This study was supported by the Natural Science Fund for Colleges and Universities in Jiangsu Province (Grant No. 20KJB460027) and the Huaian Natural Science Research Project (Grant No. HABZ201919).

References

1 Z. J. Wang, F. Chen, K. Wang, and Z. S. Wu: Ultrasonics **129** (2023) 106893. https://doi.org/10.1016/j.ultras.2022.106893
2 B. H. Tang, Y. M. Wang, A. Chen, R. Q. Gong, and Y. W. Zhao: Appl. Sci.-Basel **13** (2023) 650. https://doi.org/10.3390/app13010650
3 A. A. Eremin, M. V. Golub, S. I. Fomenko, A. A. Evdokimov, and P. A. Nets: Appl. Sci.-Basel **13** (2023) 1698. https://doi.org/10.3390/app13031698

4 M. S. Rabbi, K. Teramoto, H. Ishibashi, and M. M. Roshid: Ultrasonics **127** (2023) 106849. https://doi.org/10.1016/j.ultras.2022.106849
5 M. X. Deng, Y. X. Xiang, and L. B. Liu: J. Appl. Phys. **109** (2012) 1829. https://doi.org/10.1063/1.3592672
6 M. F. Muller , J. Y. Kim , J. M. Qu, and L. J. Jacobs: J. Acoust. Soc. Am. **127** (2010) 2141. https://doi.org/10.1121/1.3294714
7 L. A. Ostrovsky, and P. A. Johnson: Riv. Nuovo Cimento. **24** (2001) 1. https://doi.org/10.1007/BF03548898
8 P. Blanloeuil, A. Meziane, and C. Bacon: Wave Motion **51** (2013) 425. https://doi.org/10.1016/j.wavemoti.2013.10.002
9 M. Nirbhay, A. Dixit, and R. K. Misra: Materialwiss. Werkstofftech. **48** (2017) 577. https://doi.org/10.1002/mawe.201600595
10 N. D. Dushyanth, M. N. Suma, and M. V. Latte: J. Civ. Struct. Health Monit. **5** (2015) 1. https://doi.org/10.1007/s13349-015-0142-7
11 J. C. P. Allen and C. T. Ng: Compos. Struct. **311** (2023) 116805. https://doi.org/10.1016/j.compstruct.2023.116805
12 V. Aleshin and D. K. Van: J. Mech. Phys. Solids **55** (2017) 366. https://doi.org/10.1016/j.jmps.2006.07.002
13 D. Broda, W. J. Staszewski, A. Martowicz, T. Uhl, and V. V. Silberschmidt: J. Sound Vib. **33** (2014) 1097. https://doi.org/10.1016/j.jsv.2013.09.033
14 A. Zagrai and D. Donskoy: Proc. 14th AIAA/ASME/AHS Adaptive Structures Conf. (AIAA, 2006) 1–15. https://doi.org/10.2514/6.2006-2260
15 J. B. Harley: Proc. IEEE **104** (2016) 1604–1619. https://doi.org/10.1109/JPROC.2015.2481438
16 X. F. Liu, L. Bo, Y. L. Liu, Y. X. Zhao, J. Zhang, N. Hu, S. Y. Fu, and M. X. Deng: J. Sound Vib. **405** (2017) 175. https://doi.org/10.1016/j.jsv.2017.05.044
17 M. X. Deng: J. Appl. Phys. **96** (2003) 4153. https://doi.org/10.1063/1.1601312
18 F. Moser, L. J. Jacobs, and J. Qu: NDT & E Int. **32** (1999) 225. https://doi.org/10.1016/S0963-8695(98)00045-0

About the Authors

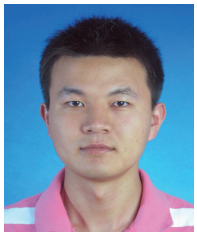

Hanfei Zhang obtained his Ph.D. degree from Shanghai University of Control Theory and Control Engineering in 2020 and is currently working at Huaiyin Normal University. His research interests include ultrasonic nondestructive detection, structural health monitoring, and signal processing. (zhanghanfei2006@163.com)

Maochao Lv graduated from China University of Mining and Technology in 2012 and is currently working at the Huai'an Measurement and Testing Center as an engineer. His research interests include fault diagnosis, health prediction, and signal processing. (270864278@qq.com)

Yanyan Luo obtained her master's degree from Liaoning University of Engineering and Technology in 2011. She is now working at Huaiyin Normal University. Her research interests include intelligent optimization, signal processing, and healthcare management optimization. (yanyanluo2008@163.com)